Time-reversed ultrasonically encoded optical focusing into scattering media

Xiao Xu, Honglin Liu and Lihong V. Wang*

Light focusing plays a central role in biomedical imaging, manipulation and therapy. In scattering media, direct light focusing becomes infeasible beyond one transport mean free path. All previous methods[1–3] used to overcome this diffusion limit lack a practical internal 'guide star'[4]. Here, we propose and experimentally validate a novel concept called time-reversed ultrasonically encoded (TRUE) optical focusing to deliver light into any dynamically defined location inside a scattering medium. First, diffused coherent light is encoded by a focused ultrasonic wave to provide a virtual internal guide star. Only the encoded light is time-reversed and transmitted back to the ultrasonic focus. The time-reversed ultrasonically encoded optical focus—defined by the ultrasonic wave—is unaffected by multiple scattering of light. Such focusing is particularly desirable in biological tissue, where ultrasonic scattering is ~1,000 times weaker than optical scattering. Various fields, including biomedical and colloidal optics, can benefit from TRUE optical focusing.

Manipulating light propagation has always been the subject of intense research[1–6]. The motivations are obvious. As the only electromagnetic wave sensitive to molecular conformation, light is an essential tool for probing the structure and properties of matter and to monitor physical, chemical or biological processes. Light (rather than harmful X-rays) is an ideal form of non-ionizing radiation for imaging and treating biological tissues. Light is also a basic tool in communications and computing. Better understanding and control of light propagation in matter has both immediate benefits and far-reaching impacts; indeed, any advance in this subject can be readily extrapolated to other fields dealing with wave phenomena[7–9].

Of particular interest is the problem of focusing light into a scattering medium. For example, high-resolution optical imaging relies on being able to precisely focus light into a medium at a desired depth. Photodynamic therapy and optogenetics require light to be delivered to specific regions of interest inside tissue. However, multiple scattering imposes a fundamental optical diffusion limit on direct light focusing in scattering media. Consequently, the imaging depth of all forms of focusing optical microscopy, such as confocal microscopy, is limited to less than one transport mean free path. A number of technologies have been developed to address this problem. For example, light can be focused through biological tissue by optical phase conjugation[3], or focused into a static scattering medium by iterative wavefront shaping, which maximizes the signal strength of a blurred yet visible implanted target[2]. However, it is desirable to focus light into (instead of through) a scattering medium, to tolerate microstructural fluctuations, and to rapidly adjust the focal position. These challenges have not been met by previous research endeavours. Our method shows great promise in addressing this need.

Our technique, called time-reversed ultrasonically encoded (TRUE) optical focusing, combines the ultrasonic modulation of diffused coherent light[10,11] with optical phase conjugation[12,13] to achieve dynamic focusing of light into a scattering medium (Fig. 1). Light from a laser source ($\lambda = 532$ nm) with long coherence length was split into three parts: a sample beam S and two mutually conjugated reference beams R and $R^\star$. S was transmitted through two acousto-optic modulators (AOM) arranged in series to tune its optical frequency to $f_S = f_0 - f_a$ before propagating diffusively through the medium (f_0 is the laser frequency and f_a the frequency shift due to the two AOMs). A focused ultrasonic wave of the same frequency f_a traversed the medium and modulated the diffused light. The ultrasonically modulated light could be regarded as emanating from a virtual source that was defined by the ultrasonic focus and was frequency-shifted by $\pm f_a$, resulting in two sidebands $S(f_\pm)$ with frequencies $f_+ = f_0$ and $f_- = f_0 - 2f_a$. This virtual source served as the internal 'guide star'[4]. Outside the medium, the diffused light was holographically recorded onto a phase-conjugate mirror, here a photorefractive $Bi_{12}SiO_{20}$ (BSO) crystal. The only stationary hologram that could be recorded was from the interference between R and $S(f_+)$[14–16]. The hologram was then read by $R^\star$ to generate a time-reversed (TR) copy of $S(f_+)$, denoted $S^\star(f_+)$. By reversibility, $S^\star(f_+)$ back-traced the trajectory of $S(f_+)$ and converged to its virtual source, thereby achieving optical focusing into the scattering medium. The energy in $S^\star(f_+)$ did not exceed
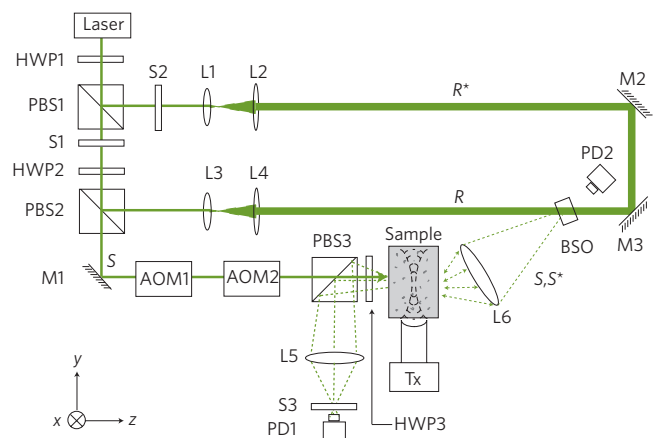

Figure 1 | Schematic of the experimental setup for TRUE optical focusing. The time-reversal procedure consisted of recording and readout of a hologram. To record a hologram, shutter S1 was opened, and S2 and S3 were closed for 190 ms; to read the hologram, S1 was closed, and S2 and S3 were opened for 10 ms. HWP*i*, *i*th halfwave plate; PBS*i*, *i*th polarizing beamsplitter; S*i*, *i*th shutter; M*i*, *i*th mirror; AOM*i*, *i*th acousto-optic modulator; L*i*, *i*th lens; PD*i*, *i*th photodiode; R, reference beam; R*, conjugated reference beam; S, signal light; S*, time-reversed signal light; BSO, $Bi_{12}SiO_{20}$; Tx, ultrasonic transducer with centre frequency $f_a = 3.5$ MHz, focal length = 38 mm, focal width = 0.87 mm. Coordinates: x = sample scanning axis, y = acoustical axis, and z = optical axis.

Optical Imaging Laboratory, Department of Biomedical Engineering, Washington University in St. Louis, St. Louis, Missouri 63130-4899, USA.
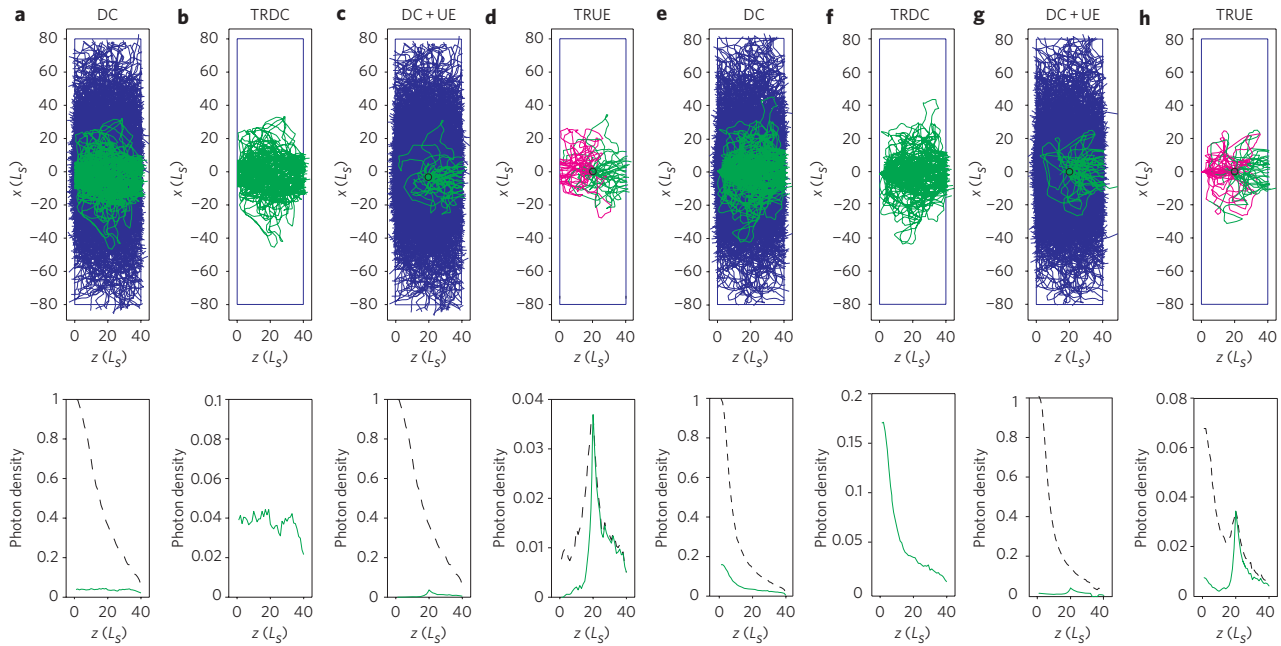*e-mail: lhwang@biomed.wustl.edu

Figure 2 | Two-dimensional Monte Carlo simulation of light propagation inside a scattering slab with dimensions $x = 160L_s$ and $z = 40L_s$. a–h, Initially, a broad (**a–d**) or narrow (**e–h**) light beam was normally incident at the origin of the coordinates. Trajectories (top panels) and photon density distribution(s) (bottom panels) along the optical axis (total density shown in dashed black) are shown. **a,e**, Diffusive trajectories of $S(f_s)$ propagating through the slab: some (shown in green) reach the phase-conjugate mirror and others (shown in blue) do not. **b,f**, Trajectories of $S^*(f_s)$ propagating back through the slab and converging to the incident point. **c,g**, Trajectories of $S(f_s)$ (shown in blue) and the ultrasonically encoded component $S(f_+)$ (shown in green) inside the slab. **d,h**, trajectories of $S^*(f_+)$ converging back to the ultrasonic focus (shown in green) then back to the incident point (shown in magenta). The black circles in the middle of the slab denote the ultrasonic focus. UE, ultrasonically encoded light.

that in $S(f_+)$ because the hologram was read without fixing. However, an intensity gain can be achieved with a higher-intensity, shorter-duration readout beam R^*. Furthermore, an energy gain much greater than unity is attainable with hologram fixing or two-step recording[14,17].

To illustrate the concept of TRUE optical focusing in a scattering medium, we used a Monte Carlo model[18] to simulate propagation of the sample light $S(f_s)$ and the ultrasonically encoded $S(f_+)$. The light–medium interaction, dominated by elastic scattering, is characterized by the scattering mean free path L_s and scattering anisotropy g. For example, $L_s \approx 0.1$ mm and $g \approx 0.9$ in human breast[19]. Optical absorption is much weaker than scattering in typical biological tissue and was neglected here. At depths beyond one transport mean free path, $L_s' = L_s/(1 - g)$, light propagation is sufficiently randomized. In our simulation, a photon was scattered ~ 70 times on average before exiting a scattering layer of thickness $L = 40L_s$. With increasing optical thickness, the intensity of the multiple-scattered light decreases much more slowly than the ballistic light, consistent with our experimental observation. The light that can be holographically recorded and time-reversed is therefore predominantly multiple-scattered.

The trajectories of $S(f_s)$, $S(f_+)$, $S^*(f_s)$ and $S^*(f_+)$ (shown in Fig. 2) appear to be random walks. However, in ideal time reversal, $S^*(f_s)$ and $S^*(f_+)$ would trace back the trajectories of $S(f_s)$ and $S(f_+)$ owing to the deterministic nature of the medium at any instant, leading to convergence to their sources (see Supplementary Videos). Without ultrasonic encoding, $S^*(f_s)$ converged to the incident location of $S(f_s)$. With ultrasonic encoding, $S^*(f_+)$ converged to the ultrasonic focus instead, which is the source of $S(f_+)$.

TRUE optical focusing was then validated with imaging experiments (Fig. 3). The imaging sample was a 10-mm-thick scattering slab, made from a mixture of porcine gelatine, distilled water and 0.25% Intralipid, resulting in $L_s \approx 0.4$ mm, $g \approx 0.9$ and absorption

length $L_a \approx 79$ mm. The light beam initially had a diameter of 2 mm on the incident plane of the sample and diffused to ~ 4 mm (FWHM) in the middle plane, which contained three objects with different compositions: two dyed with black ink (Obj1 and Obj2), resulting in an optical absorption coefficient $\mu_a \approx 0.8$ mm^{-1}, and one having 1% concentration Intralipid (Obj3), resulting in $L_s \approx 0.1$ mm. When the sample was laterally scanned along the x-axis, four one-dimensional images were acquired (Fig. 3b,c). The first two were acquired without either AOM tuning or ultrasonic modulation. To form the first image (a direct current (DC) image), $S(f_s)$ was detected by a photodiode at the BSO position. To form the second image (a time-reversed direct current (TRDC) image), $S^*(f_s)$ was transmitted back through the sample and detected by a photodiode PD1. To form the third image (a 'UOT' image based on conventional ultrasound-modulated optical tomography (UOT)[15,16]), $S(f_+)$ was spectrally filtered by the BSO and then detected by PD2. To form the fourth image (a 'TRUE' image), $S^*(f_+)$ was transmitted back through the sample and detected by PD1.

The salient differences in the apparent image resolution and contrast among the four imaging methods stem from the distinct inherent imaging mechanisms. The DC and TRDC imaging methods, suffering from optical diffusion, lacked the spatial resolution to resolve the three objects. The optical diffusion, approximated as a Gaussian profile, was convolved with the object profile to fit the experimental data. The full-widths at half-maxima (FWHMs) of the Gaussian profiles, defined as the image resolutions, were 3.4 mm for DC imaging and 3.2 mm for TRDC imaging. In contrast, the UOT and TRUE imaging methods, based on imaging signals emanating from the internal virtual sources, both adequately depicted the profiles of the objects. The ultrasonic focus, approximated as a Gaussian profile, was convolved with the object profile to fit the data. The resolutions were 0.89 mm and 0.63 mm for UOT and TRUE imaging, respectively.
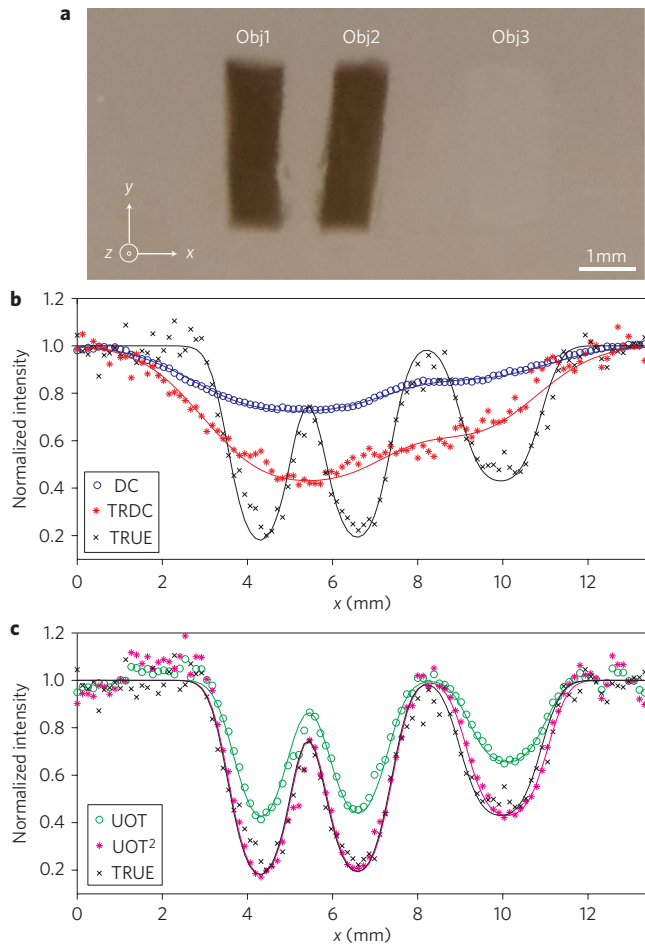
155

Figure 3 | Results from four imaging experiments validating TRUE optical focusing. a, Photograph of the imaged sample dissected at the middle plane containing two absorbing objects (Obj1 and Obj2) and one scattering object (Obj3). The object dimensions were $x = 1.3$ mm, $y = 4.5$ mm and $z = 1$ mm for the two absorbing objects and $x = 1.7$ mm, $y = 4.5$ mm and $z = 0.6$ mm for the scattering object. The full dimensions of the sample were $x = y = 60$ mm and $z = 10$ mm. **b**, Comparison of the normalized DC, TRDC and TRUE images of the sample. The absolute strengths of the TRDC and TRUE signals were ~3,000 mV and ~30 mV, respectively. The objects could not be distinguished in the DC and TRDC images, but in the TRUE image the objects were clearly shown against the background with 61% contrast for the absorbing objects and 31% contrast for the scattering object. **c**, Comparison of the UOT and TRUE images of the sample to demonstrate the square law: the TRUE signal is proportional to the square of the UOT signal (UOT^2). The FWHMs of the pointspread functions were 0.89 mm (UOT) and 0.63 mm (TRUE), the ratio of which is 1.4 (~$\sqrt{2}$). In **b** and **c**, symbols represent experimental data and solid curves represent Gaussian fits.

A square law exists if $S^\star(f_+)$ indeed converges to the ultrasonic focus: the TRUE signal is proportional to the square of the UOT signal. On the one hand, the optical field for the UOT image is given by $S(x, f_+)|_{BSO} \propto C(x) \cdot S_{in}(f_s)$, where $C(x)$ is a virtual source term and $S_{in}(f_s)$ is the incident optical field. On the other hand, for the TRUE image, $S^\star(x, f_+)|_{BSO} \propto S(x, f_+)|_{BSO}$. As $S^\star(f_+)$ inversely traverses the sample, the virtual source term in its conjugated form $C^\star(x)$ operates on $S^\star(x, f_+)|_{BSO}$. As a result, the optical field detected by PD1 is $S^\star(x, f_s)|_{PD1} \propto C^\star(x) \cdot S^\star(x, f_+)|_{BSO} \propto |C(x)|^2 \cdot S_{in}(f_s)$. Therefore, the detected light intensities in UOT and TRUE imaging are related by $|S^\star(x, f_s)|_{PD1}|^2 \propto |S(x, f_+)|_{BSO}|^4$. This prediction was verified by the normalized amplitudes of the UOT and TRUE images in Fig. 3c. Furthermore, if the pointspread

functions in UOT and TRUE imaging follow Gaussian profiles, their widths—defining the spatial resolutions—have a $\sqrt{2}$:1 ratio. This second prediction agrees with the ratio of 1.4 between the image resolutions of UOT (0.89 mm) and TRUE (0.63 mm) imaging. In addition, the resolution of UOT is in agreement with the ultrasonic focal diameter of 0.87 mm.

Focusing into a scattering medium is much more valuable than focusing through it. In fact, the former can be reduced to the latter by moving the focal position. Focusing through a medium is used to image a target outside a scattering medium, which can be either viewed directly from the target side or scanned by a collimated laser beam. Focusing into the medium must be used to image or treat a target embedded inside a scattering medium. For example, when a tumour inside biological tissue is optically imaged or treated, light must be focused to the tumour.

Focusing light into a scattering medium dynamically, with the desired speed and localization, can profoundly benefit studies involving photophysical, photochemical and photobiological processes. This work has demonstrated the feasibility of TRUE optical focusing by combining two key mechanisms—localized ultrasonic encoding of the diffused light and selective time reversal of the encoded light—to suppress the scattering effect. The focal spot size can be flexibly scaled with the ultrasonic frequency, and the experimental system can be adapted for reflection or other configurations according to the application. Improvement can be made by using faster photorefractive materials, time-reversal techniques with energy gains greater than unity, and more efficient time-reversal configurations. TRUE optical focusing—effectively bringing order to the chaotic scattering process—has potential in imaging technologies (such as fluorescence microscopy, diffuse optical tomography and photoacoustic tomography), manipulation technologies (such as optical tweezers and optogenetics), and therapeutic technologies (such as photodynamic and photothermal therapies).

References

1. Vellekoop, I. M. & Mosk, A. P. Focusing coherent light through opaque strongly scattering media. *Opt. Lett.* **32**, 2309–2311 (2007).
2. Vellekoop, I. M., van Putten, E. G., Lagendijk, A. & Mosk, A. P. Demixing light paths inside disordered metamaterials. *Opt. Express* **16**, 67–80 (2008).
3. Yaqoob, Z., Psaltis, D., Feld, M. S. & Yang, C. H. Optical phase conjugation for turbidity suppression in biological samples. *Nature Photon.* **2**, 110–115 (2008).
4. Primmerman, C. A., Murphy, D. V., Page, D. A., Zollars, B. G. & Barclay, H. T. Compensation of atmospheric optical distortion using a synthetic beacon. *Nature* **353**, 141–143 (1991).
5. Popoff, S. M. *et al.* Measuring the transmission matrix in optics: an approach to the study and control of light propagation in disordered media. *Phys. Rev. Lett.* **104**, 100601 (2010).
6. Vellekoop, I. M., Lagendijk, A. & Mosk, A. P. Exploiting disorder for perfect focusing. *Nature Photon.* **4**, 320–322 (2010).
7. Ishimaru, A. *Wave Propagation and Scattering in Random Media* (Academic Press, 1978).
8. Fink, M. *et al.* Time-reversed acoustics. *Rep. Prog. Phys.* **63**, 1933–1995 (2000).
9. Lerosey, G., De Rosny, J., Tourin, A. & Fink, M. Focusing beyond the diffraction limit with far-field time reversal. *Science* **315**, 1120–1122 (2007).
10. Mahan, G. D., Engler, W. E., Tiemann, J. J. & Uzgiris, E. Ultrasonic tagging of light: theory. *Proc. Natl Acad. Sci. USA* **95**, 14015–14019 (1998).
11. Wang, L. H. V. Mechanisms of ultrasonic modulation of multiply scattered coherent light: an analytic model. *Phys. Rev. Lett.* **87**, 043903 (2001).
12. Gunter, P. Holography, coherent-light amplification and optical-phase conjugation with photorefractive materials. *Phys. Rep.* **93**, 199–299 (1982).
13. He, G. S. Optical phase conjugation: principles, techniques, and applications. *Prog. Quantum Electron.* **26**, 131–191 (2002).
14. Solymar, L., Webb, D. J. & Grunnet-Jepsen, A. *The Physics and Applications of Photorefractive Materials* (Clarendon Press, 1996).
15. Ramaz, F. *et al.* Photorefractive detection of tagged photons in ultrasound modulated optical tomography of thick biological tissues. *Opt. Express* **12**, 5469–5474 (2004).
16. Xu, X. *et al.* Photorefractive detection of tissue optical and mechanical properties by ultrasound modulated optical tomography. *Opt. Lett.* **32**, 656–658 (2007).

17. Gunter, P. & Huignard, J. P. *Photorefractive Materials and Their Applications. 1 Basic Effects* (Springer, 2006).
18. Wang, L. V., Jacques, S. L. & Zheng, L. Q. MCML—Monte Carlo modeling of photon transport in multi-layered tissues. *Comput. Methods Programs Biomed.* **47,** 131–146 (1995).
19. Srinivasan, S. *et al*. Interpreting hemoglobin and water concentration, oxygen saturation, and scattering measured *in vivo* by near-infrared breast tomography. *Proc. Natl Acad. Sci. USA* **100,** 12349–12354 (2003).

Author contributions

X.X. and H.L. contributed equally to the experimental design and study, Monte Carlo simulation, data analysis and writing of the manuscript. L.W. conceived the original idea, discussed the experiments and revised the paper.

Additional information

The authors declare competing financial interests: details accompany the full-text HTML version of the paper at www.nature.com/naturephotonics. Supplementary information accompanies this paper at www.nature.com/naturephotonics. Reprints and permission information is available online at http://npg.nature.com/reprintsandpermissions/. Correspondence and requests for materials should be addressed to L.V.W.